RESEARCH ARTICLE

CFD Modeling of Fire

An overview of a methodology for simulating fires and other thermally-driven, low-speed flows is presented. The model employs a number of simplifications of the governing equations that allow for relatively fast simulations of practical fire scenarios. The hydrodynamic model consists of the low Mach number large-eddy simulation subgrid closure with either a constant or dynamic coefficient eddy diffusivity. Combustion is typically treated as a mixing-controlled, single-step reaction of fuel and oxygen. The radiation transport equation is written in terms of a spectrally-averaged gray gas. Applications of the model include the design of fire protection systems in buildings and the reconstruction of actual fires.

2

1
2
3
4
5
6
7
8
9
10
11
12
13
14
15
16
17
18
19
20
21
22
23
24
25
26
27
28
29
30
31
32
33
34
35
36
37
38
39
40
41
42
43
44
45
46
47
48
49
50
51
52
53
54
55
56
57
58
59
60

1. Nomenclature

c_p	constant pressure specific heat
D_α	diffusion coefficient of species α
D	fire diameter
$\mathbf{f}_b$	external force vector (excluding gravity)
$\mathbf{g}$	gravity vector
$\mathcal{H}$	stagnation pressure per unit mass
h_s	specific enthalpy
I	radiation intensity
I_b	radiation black body intensity
k	thermal conductivity
k_{sgs}	subgrid-scale turbulent kinetic energy
$\dot{m}'''_{b,\alpha}$	mass production rate of species α by evaporating droplets/particles
$\dot{m}'''_\alpha$	mass production rate of species α per unit volume
p	pressure
$\bar{p}$	background pressure
$\tilde{p}$	pressure perturbation
$\dot{q}'''$	heat release rate per unit volume
$\dot{\mathbf{q}}''_r$	radiative heat flux vector
$\dot{Q}$	total heat release rate
Q^*	fire Froude number
$\mathcal{R}$	universal gas constant
$\mathbf{s}$	unit vector in direction of radiation intensity
Sc_t	turbulent Schmidt number
T	temperature
t	time
U	integrated radiant intensity
$\mathbf{u}$	velocity vector
W_α	molecular weight of gas species α
$\overline{W}$	molecular weight of the gas mixture
$\mathbf{x} = (x, y, z)$	position vector
Y_α	mass fraction of primitive species α
Z_α	mass fraction of lumped species α
Δ	large-eddy simulation filter width
ΔH	heat of combustion
κ	absorption coefficient
μ	dynamic viscosity
ν_α	stoichiometric coefficient of species α
ρ	density
τ	mixing time
$\boldsymbol{\tau}$	viscous stress tensor
χ_r	radiative loss fraction
σ	Stefan-Boltzmann constant
$\boldsymbol{\omega}$	vorticity vector

1
2
3
4
5
6
7
8
9
10
11
12
13
14
15
16
17
18
19
20
21
22
23
24
25
26
27
28
29
30
31
32
33
34
35
36
37
38
39
40
41
42
43
44
45
46
47
48
49
50
51
52
53
54
55
56
57
58
59
60

2. Introduction

The idea that the dynamics of a fire might be studied numerically dates back to the beginning of the computer age. Indeed, the fundamental conservation equations governing fluid dynamics, heat transfer, and combustion were first written down over a century ago. Despite this, practical mathematical models of fire (as distinct from controlled combustion) are relatively recent due to the inherent complexity of the problem. Indeed, in his brief history of the early days of fire research, Hoyt Hottel noted "A case can be made for fire being, next to the life processes, the most complex of phenomena to understand" (Hottel 1984).

The difficulties revolve about three issues: First, there are an enormous number of possible fire scenarios to consider. Second, the physical insight and computing power for realistic fire scenarios are limited. Finally, the "fuel" in most fires was never intended as such. Thus, the mathematical models and the data needed to characterize the degradation of the condensed phase materials that supply the fuel may not be available.

In order to make progress, the questions that are asked have to be greatly simplified. To begin with, instead of seeking a methodology that can be applied to all fire problems, we begin by looking at a few scenarios that seem to be most amenable to analysis. Hopefully, the methods developed to study these "simple" problems can be generalized over time so that more complex scenarios can be analyzed. Second, we must learn to live with idealized descriptions of fires and approximate solutions to our idealized equations. Finally, the methods should be capable of systematic improvement. As our physical insight and computing power grow more powerful, the methods of analysis can grow with them.

Models specifically designed to study the impact of fire on buildings emerged in the 1970s. The first models were essentially empirical correlations that provided estimates of plume and compartment temperatures, heat flux, and smoke concentration. These correlations were then incorporated into what became known as "zone" models, in which each compartment is divided into two spatially homogeneous volumes, a hot upper layer and a cooler lower layer (Jones 1983, Quintiere 1984). This choice of model was driven in large part by the capabilities of computer hardware of that time. In these models, mass and energy balances are enforced for each layer, with additional models describing other physical processes appended as differential or algebraic equations as appropriate. The relative physical and computational simplicity of the zone models has led to their widespread use in the analysis of fire scenarios. Provided that the two layer assumption is valid and that detailed spatial resolution is not required, these models are quite reliable. However, by their very nature, there is no way to systematically improve them. The rapid growth of computing power and the corresponding maturing of computational fluid dynamics (CFD), has led to the development of CFD based "field" models applied to fire research problems. Virtually all this work is based on the conceptual framework provided by the Reynolds-averaged form of the Navier-Stokes equations (RANS), in particular the $k-\epsilon$ turbulence model pioneered by Patankar (1980). The use of CFD models has allowed the description of fires in complex geometries, and the incorporation of a wide variety of physical phenomena. However, these models have a fundamental limitation for fire applications—the averaging procedure at the root of the model equations.

RANS models were developed as a time-averaged approximation to the conservation equations of fluid dynamics. While the precise nature of the averaging time is not specified, it is clearly long enough to require the introduction of large-eddy transport coefficients to describe the unresolved fluxes of mass, momentum and energy. Unfortunately,

4

1
2
3
4
5
6
7
8
9
10
11
12
13
14
15
16
17
18
19
20
21
22
23
24
25
26
27
28
29
30
31
32
33
34
35
36
37
38
39
40
41
42
43
44
45
46
47
48
49
50
51
52
53
54
55
56
57
58
59
60

the evolution of large-eddy structures characteristic of most fire plumes is lost with such an approach, as is the prediction of local transient events. It is sometimes argued that the averaging process used to define the equations is an "ensemble average" over many replicates of the same experiment or postulated scenario. However, this is a moot point in fire research since neither experiments nor real scenarios are replicated in the sense required by that interpretation of the equations. The application of large-eddy simulation (LES) techniques to fire is aimed at extracting greater temporal and spatial fidelity from simulations of fire performed on the more finely meshed grids allowed by ever faster computers.

The phrase LES refers to the description of turbulent mixing of the gaseous fuel and combustion products with the local atmosphere surrounding the fire. This process, which determines the burning rate in most fires and controls the spread of smoke and hot gases, is extremely difficult to predict accurately. This is true not only in fire research but in almost all phenomena involving turbulent fluid motion. The basic idea behind the LES technique is that the eddies that account for most of the mixing are large enough to be calculated with reasonable accuracy from the equations of fluid dynamics. The hope (which must ultimately be justified by comparison to experiments) is that small-scale eddy motion can be modeled.

The general equations of fluid dynamics describing the transport of mass, momentum, and energy by fire-induced flows must be simplified so that they can be solved efficiently. The simplified equations, developed by Rehm and Baum (1978), have been widely adopted by the larger combustion research community, where they are referred to as the "low Mach number" combustion equations. They describe the low speed motion of a gas driven by chemical heat release and buoyancy forces. Oran and Boris (1987) provide a useful discussion of the technique as applied to various reactive flow regimes. They comment that "There is generally a heavy price for being able to use a single algorithm for both fast and slow flows, a price that translates into many computer operations per time step often spent in solving multiple and complicated matrix operations."

The basic low Mach number framework pioneered by Rehm and Baum in the early 1980s has evolved to become an open source fire model known as the Fire Dynamics Simulator (FDS) (McGrattan *et al.* 2007b). It was released in 2000, and is currently used by fire researchers and fire protection engineers for a wide variety of applications. The software can run either on a single processor personal computer or it can operate over multiple computers using Message Passing Interface (MPI). Desktop computers limit the number of cells to at most a few million. This means that the ratio of largest to smallest eddy length scales that can be resolved by the computation (the "dynamic range" of the simulation) is on the order of 100. Parallel processing can be used to extend this range to some extent, but the range of length scales that need to be accounted for if all relevant fire processes are to be simulated is roughly 10^4 to 10^5 because combustion processes take place at length scales of 1 mm or less, while the length scales associated with building fires are of the order of tens of meters. The form of the numerical equations discussed below depends on which end of the spectrum one wants to capture directly, and which end is to be ignored or approximated.

The remainder of this paper describes the basic methodology of FDS, an example of its validation process, and a few practical applications.

3. Model Overview

This section presents the governing equations of FDS and an outline of the general solution procedure. Details are presented in the technical documentation of the model (McGrattan *et al.* 2007b). The purpose of this chapter is to highlight aspects of the solution methodology that make it practical for thermally-driven flow simulations, in particular fire. Some of the major features of the model, in its default operation, are:

- Low Mach, large-eddy simulation (LES)
- Explicit, second-order, energy conserving numerics
- Structured, uniform, staggered grid
- Simple immersed boundary method for treatment of flow obstructions
- Generalized "lumped species" method (simplified reaction progress variable approach)
- Smagorinsky subgrid closure (constant or dynamic coefficient)
- Constant turbulent Schmidt and Prandtl numbers
- Eddy dissipation model (fast chemistry) for single-step reaction between fuel and oxidizer
- Gray gas radiation with finite volume solution to the radiation transport equation, including absorption and scattering by droplets
- Coupled heat transfer on solid surfaces

The model, however, is not limited to these simple algorithms. For example, the user may specify multiple reactions, finite-rate chemistry, a wide-band radiation model, and a variety of other special features. The more detailed physics incur increased computational cost and it is incumbent on the user to justify the added expense in terms of improved accuracy. The default model options have been selected based on results from a wide variety of full-scale validation experiments (McGrattan *et al.* 2007a).

The algorithm outlined below has evolved over roughly three decades. Initially, it was designed to study buoyant plumes in the Boussinesq limit; that is, the fluid was assumed incompressible but included a source term for buoyancy. This approach was based on a long tradition in fire research of modeling smoke movement using dyed salt water introduced into a tank filled with fresh water. Eventually, this approach proved too limiting, but some of the major features of the algorithm, like the low Mach number approximation, were retained.

3.1. *LES Formalism*

The equations for large-eddy simulation (LES) are derived by applying a low-pass filter, parameterized by a width Δ, to the transport equations for mass, momentum and energy. For our purposes, it is sufficient to think of the filtered fields in the LES equations as cell means. For example, in one dimension the filtered density, $\bar{\rho}(x,t)$, for a cell of width Δ is

$$\bar{\rho}(x,t) = \frac{1}{\Delta} \int_{x-\Delta/2}^{x+\Delta/2} \rho(r,t)\,\mathrm{d}r. \tag{1}$$

In FDS, the filter width Δ is equivalent to the local cell size, δx, and is a key parameter in the submodels for the turbulent viscosity and the reaction time scale discussed later. The practice of taking $\Delta = \delta x$ is called implicit filtering. In what follows, the filter formalism is relaxed (the overline notation is suppressed for clarity) since no explicit filtering oper-

6

ations are performed in the algorithm except within the dynamic procedure (Germano
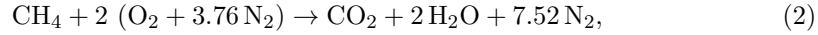*et al.* 1991).

3.2. *Numerical Grid*

FDS is designed to be used by practicing engineers for a variety of fire protection and
other thermal flow applications. Therefore, it must be relatively fast and robust, and it
must be easy to describe the scenario. This means that the user should only have to spec-
ify a small number of numerical parameters, focusing instead on the physical description
of the problem. Because the computational domain usually encompasses a volume within
a building, or the entire building itself, the most obvious and simplest numerical grid is
rectilinear. In fact, because FDS is an LES model, uniform meshing is preferred, and the
only numerical parameters chosen by the end user are the three dimensions of the grid.
Once established, it is relatively simple to define rectangular obstructions that define the
geometry to the level of resolution determined by the grid. These obstructions "snap" to
the underlying grid, an elementary form of immersed boundary method (IBM).

   The governing equations are approximated using second-order accurate finite differ-
ences on a collection of uniformly spaced three-dimensional grids. Multiple meshes can
be processed in parallel using Message Passing Interface (MPI) libraries. Scalar quantities
are assigned to the center of each grid cell; vector components are assigned at the appro-
priate cell faces. This is what is commonly referred to as a staggered grid (Harlow and
Welch 1965). Its main purpose is to avoid numerical dispersion error (checker-boarding)
in pressure-velocity coupling by naturally representing the pressure cell velocity diver-
gence, a very important thermodynamic quantity in the model.

3.3. *Mass and Species Transport*

The most basic description of the chemistry of fire is a reaction of a hydrocarbon fuel
with oxygen that produces carbon dioxide and water vapor. Because fire is a relatively
inefficient combustion process involving multiple fuel gases that contain more than just
carbon and hydrogen atoms, the number of gas species to track in the simulation could be
large if detailed chemistry is employed. However, to make the simulations tractable, we
limit the number of fuels to one, usually, and the number of reactions to just one or two.
We also leave open the possibility that the reaction may not proceed for lack of sufficient
oxygen in the incoming air stream, as when a fire in a closed compartment extinguishes
itself. This simplified approach to the chemistry still involves at least six gas species
(Fuel, O_2, CO_2, H_2O, CO, N_2) plus soot particulate. If we assume a single-step reaction,
we do not need to solve explicitly seven transport equations. We only need to solve
two: one for the fuel and one for the products. Air is everything that is neither fuel nor
products. Whereas the fuel is a single gas species, the air and products are referred to as
"lumped species". A lumped species represents a mixture of gas species that are created,
transported, or destroyed *en masse* (*i.e.* the lumped species has a single set of transport
properties), and from the point of view of the numerical model it can thus be treated
as a single species. In fact, the mass transport equations make no distinction between a
single or lumped species. For example, air is a lumped species that consists of nitrogen,
oxygen, and trace amounts of water vapor and carbon dioxide. We use the symbols Z_A,
Z_F, and Z_P to denote the mass fractions of air, fuel, and products ($Z_A = 1 - Z_F - Z_P$).
The lumped species mass fractions are linearly related to the primitive species mass
fractions, Y_α; thus, conversion from one to the other is a simple matter of performing a

1
2
3
4
5
6
7
8
9
10
11
12
13
14
15
16
17
18
19
20
21
22
23
24
25
26
27
28
29
30
31
32
33
34
35
36
37
38
39
40
41
42
43
44
45
46
47
48
49
50
51
52
53
54
55
56
57
58
59
60

matrix multiplication. For example, the complete combustion of methane,

$$CH_4 + 2\,(O_2 + 3.76\,N_2) \rightarrow CO_2 + 2\,H_2O + 7.52\,N_2, \tag{2}$$

is expressed as

$$Fuel + 2\,Air \rightarrow Products, \tag{3}$$

and the primitive species can be recovered from the lumped species via

$$\begin{bmatrix} Y_{N_2} \\ Y_{O_2} \\ Y_{CH_4} \\ Y_{CO_2} \\ Y_{H_2O} \end{bmatrix} = \begin{bmatrix} 0.77 & 0.00 & 0.73 \\ 0.23 & 0.00 & 0.00 \\ 0.00 & 1.00 & 0.00 \\ 0.00 & 0.00 & 0.15 \\ 0.00 & 0.00 & 0.12 \end{bmatrix} \begin{bmatrix} Z_A \\ Z_F \\ Z_P \end{bmatrix}. \tag{4}$$

The lumped species approach does not change the basic mass transport equations. The equation for total mass is written:

$$\frac{\partial \rho}{\partial t} + \nabla \cdot (\rho \mathbf{u}) = \dot{m}_b'''. \tag{5}$$

Note that the source term on the right hand side represents the addition of mass from evaporating droplets or other subgrid-scale particles that represent sprinkler and fuel sprays, vegetation, and any other type of small, unresolvable object. These objects are assumed to occupy no volume; thus, they are treated within the governing equations as point sources of mass, momentum and energy.

The transport equation for each of the lumped species minus one (usually air) has the same form as the transport equation for a single species:

$$\frac{\partial}{\partial t}(\rho Z_\alpha) + \nabla \cdot (\rho Z_\alpha \mathbf{u}) = \nabla \cdot (\rho D_\alpha \nabla Z_\alpha) + \dot{m}_\alpha''' + \dot{m}_{b,\alpha}'''. \tag{6}$$

Here $\dot{m}_b''' = \sum_\alpha \dot{m}_{b,\alpha}'''$ is the production rate of species by evaporating droplets or particles. Summing these equations over all species yields the original mass conservation equation because $\sum Z_\alpha = 1$ and $\sum \dot{m}_\alpha''' = 0$ and $\sum \dot{m}_{b,\alpha}''' = \dot{m}_b'''$, by definition, and because it is assumed that $\sum \rho D_\alpha \nabla Z_\alpha = 0$. This last assertion is not true, in general. However, transport equations are solved for total mass and all but one of the species, implying that the diffusion coefficient of the implicit species is chosen so that the sum of all the diffusive fluxes is zero.

3.4. *Low Mach Number Approximation*

Rehm and Baum (1978) observed that for low speed applications like fire, the spatially and temporally resolved pressure, p, can be decomposed into a "background" pressure, $\overline{p}(z,t)$, plus a perturbation, $\tilde{p}(x,y,z,t)$, with only the background pressure retained in the equation of state:

$$\overline{p} = \rho T \mathcal{R} \sum_\alpha \frac{Z_\alpha}{W_\alpha} \equiv \frac{\rho \mathcal{R} T}{\overline{W}}. \tag{7}$$

8

Note that z is the spatial coordinate in the direction of gravity; thus, the stratification of the atmosphere is included in the background pressure. The perturbation, $\tilde{p}$, drives the fluid motion. This approximation has a number of consequences. First, building compartments connected via a heating, ventilation, and air conditioning system can each maintain individual background pressures. The air flows between compartments can be described in terms of the differences in the background pressures, eliminating the need to solve detailed flow equations within the ventilation ducts.

The second consequence of the low Mach number approximation is that it eliminates the need to solve the energy transport equation explicitly. The energy conservation equation is written in terms of the *sensible enthalpy*, h_s:

$$\frac{\partial}{\partial t}(\rho h_s) + \nabla \cdot (\rho h_s \mathbf{u}) = \frac{\mathrm{D}p}{\mathrm{D}t} + \dot{q}''' - \dot{q}'''_b + \nabla \cdot k\nabla T + \nabla \cdot \sum_\alpha h_{s,\alpha} \rho D_\alpha \nabla Z_\alpha - \nabla \cdot \dot{\mathbf{q}}''_r. \quad (8)$$

Note that the material derivative of the thermodynamic pressure is simplified because of the low Mach number approximation:

$$\frac{\mathrm{D}p}{\mathrm{D}t} \equiv \frac{\partial p}{\partial t} + \mathbf{u} \cdot \nabla p \approx \frac{\partial \overline{p}}{\partial t} + w \frac{\partial \overline{p}}{\partial z}. \quad (9)$$

The term, $\dot{q}'''$, is the heat release rate per unit volume from a chemical reaction, *i.e.* the fire. The term, $\dot{q}'''_b$, is the energy transferred to subgrid-scale droplets and particles. The term, $\nabla \cdot \dot{\mathbf{q}}''_r$, is the net absorption and emission of thermal radiation.

As mentioned above, we do not actually solve Eq. (8). Instead, we form an expression for the divergence of the velocity starting with the mass conservation equation (5), and then take the material derivative of the equation of state (7):

$$\nabla \cdot \mathbf{u} = \frac{1}{\rho}\left(\dot{m}'''_b - \frac{\mathrm{D}\rho}{\mathrm{D}t}\right) = \frac{1}{\rho}\dot{m}'''_b - \frac{1}{\overline{p}}\frac{\mathrm{D}\overline{p}}{\mathrm{D}t} + \overline{W}\frac{\mathrm{D}}{\mathrm{D}t}\left(\frac{1}{\overline{W}}\right) + \frac{1}{T}\frac{\mathrm{D}T}{\mathrm{D}t}. \quad (10)$$

Expanding the material derivatives on the right hand side of this equation produces a fairly complicated expression for the divergence that includes the source and diffusion terms from the mass, species, and energy conservation equations. However, its importance to the overall algorithm is that it can be computed using only the thermodynamic variables ρ, Z_α, and $\overline{p}$. As will be shown below, the way to advance the flow velocity in time is to first estimate the thermodynamic variables at the next time step, compute the divergence, and then solve an equation for the pressure that will guarantee that the divergence of the updated velocity is identical to that computed solely from the thermodynamic variables.

3.5. *Momentum Transport*

Noting the vector identity $(\mathbf{u}\cdot\nabla)\mathbf{u} = \nabla|\mathbf{u}|^2/2 - \mathbf{u}\times\boldsymbol{\omega}$ and defining the stagnation pressure per unit mass $\mathcal{H} \equiv |\mathbf{u}|^2/2 + \tilde{p}/\rho$, the momentum equation can be written as:

$$\frac{\partial \mathbf{u}}{\partial t} - \mathbf{u}\times\boldsymbol{\omega} + \nabla\mathcal{H} - \tilde{p}\nabla\left(\frac{1}{\rho}\right) = \frac{1}{\rho}\Big[(\rho - \rho_0)\mathbf{g} + \mathbf{f}_b + \nabla\cdot\boldsymbol{\tau}\Big]. \quad (11)$$

The term, $\mathbf{f}_b$, represents the drag force exerted by the subgrid-scale particles and droplets. The viscous stress, $\boldsymbol{\tau}$, is closed via gradient diffusion with the turbulent viscosity obtained

from the Smagorinsky model (constant or dynamic coefficient) (Germano *et al.* 1991, Moin *et al.* 1991, Smagorinsky 1963).

It is convenient to write this equation in the form:

$$\frac{\partial \mathbf{u}}{\partial t} + \mathbf{F} + \nabla \mathcal{H} = 0. \tag{12}$$

so that a Poisson equation for the pressure can be derived by taking its divergence:

$$\nabla^2 \mathcal{H} = -\frac{\partial}{\partial t}(\nabla \cdot \mathbf{u}) - \nabla \cdot \mathbf{F}. \tag{13}$$

Note the appearance of the time derivative of the divergence. This is an important feature of the time marching scheme. Note also that the right hand side of the Poisson equation retains a term that includes the perturbation pressure, $\tilde{p}\nabla(1/\rho)$. This term accounts for the baroclinic torque. It is included on the right hand side of the Poisson equation by using its value from the previous time step. This approximation allows us to solve a separable form of the Poisson equation, for which there are fast, direct solvers that are optimized for uniform grids (Sweet 1973).

3.6. *Combustion, Radiation, and Surface Heat Transfer*

Combustion and radiation are introduced into the governing equations via the source terms, $\dot{q}'''$ and $\nabla \cdot \mathbf{q}''_r$, in the energy transport equation. Since the energy equation is not solved explicitly, these terms find their way into the expression for the divergence.

3.6.1. *Combustion*

For most applications, FDS uses a combustion model based on the mixing-limited, infinitely fast reaction of lumped species. The reaction of fuel and oxygen is not necessarily instantaneous and complete, and there are several optional schemes that are designed to predict the extent of combustion in under-ventilated spaces.

For an infinitely fast reaction, reactant species in a given grid cell are converted to product species at a rate determined by a characteristic mixing time. If any grid cell contains all the reactants of the the chemical reaction and the mass fractions of reactants and products meet certain criteria, the heat release rate per unit volume is given by the eddy dissipation model (Magnussen and Hjertager 1977, Poinsot and Veynante 2005)

$$\dot{q}''' \equiv -\dot{m}_f''' \Delta H = -\rho \min\left(Y_{\mathrm{F}}, \frac{Y_{\mathrm{O}_2}}{s}, \beta\frac{Y_{\mathrm{P}}}{1+s}\right)\left(1 - e^{-\delta t/\tau_{mix}}\right)\Delta H \quad ; \quad s = \frac{W_{\mathrm{F}}}{\nu_{\mathrm{O}_2} W_{\mathrm{O}_2}}. \tag{14}$$

Here, Y_{F}, Y_{O_2}, and Y_{P} are the mass fractions of fuel, oxygen and products within a grid cell; β is an empirical parameter. The mixing time τ_{mix} is given by

$$\tau_{mix} = \max(\tau_{chem}, \min(\tau_d, \tau_u, \tau_g, \tau_{flame})). \tag{15}$$

where

$$\tau_d = \frac{\mathrm{Sc}_t\rho\Delta^2}{\mu} \;\; ; \quad \tau_u = \frac{\Delta}{\sqrt{2k_{sgs}}} \;\; ; \quad \tau_g = \sqrt{\frac{2\Delta}{g}}. \tag{16}$$

10

Note that k_{sgs} is the subgrid kinetic energy per unit mass which is closed by integrating a model Kolmogorov spectrum. The acceleration time scale τ_g is the time required to travel a distance Δ starting from rest under a constant acceleration, $g = 9.81$ m/s^2. The chemistry time scale τ_{chem} (usually very small) and the flame time scale τ_{flame} (usually very large) are physical limits on the mixing time which may be adjusted if necessary by the user.

3.6.2. Radiation

The net contribution from thermal radiation in the energy equation is defined by:

$$-\nabla \cdot \dot{\mathbf{q}}_r''(\mathbf{x}) = \kappa(\mathbf{x})\,[U(\mathbf{x}) - 4\pi\,I_b(\mathbf{x})] \quad ; \quad U(\mathbf{x}) = \int_{4\pi} I(\mathbf{x}, \mathbf{s}')\,d\mathbf{s}' \tag{17}$$

where $\kappa(\mathbf{x})$ is the absorption coefficient, $I_b(\mathbf{x})$ is the source term, and $I(\mathbf{x}, \mathbf{s})$ is the solution of the radiation transport equation (RTE) for a non-scattering gray gas:

$$\mathbf{s} \cdot \nabla I(\mathbf{x}, \mathbf{s}) = \kappa(\mathbf{x})\,[I_b(\mathbf{x}) - I(\mathbf{x}, \mathbf{s})]. \tag{18}$$

In practical simulations, the spectral dependence of I, I_b, and κ cannot be resolved accurately, nor do we have reliable data for non-ideal fuels typical of real fires. While FDS does have an option to divide the radiation spectrum into a relatively small number of bands and solve a separate RTE for each band, it is usually not necessary because in real fires, soot is the dominant source and sink of thermal radiation and is not particulary sensitive to wavelength. The mean absorption coefficient, κ, is a function of species composition and temperature. Its values are obtained by table look-up using a narrow-band model, RadCal (Grosshandler 1993).

Although soot-laden gases are assumed to be non-scattering, water droplets can absorb and scatter thermal radiation. This is important in cases involving mist sprinklers, but also plays a role in all sprinkler cases. The absorption and scattering coefficients are based on Mie theory.

The source term, I_b, requires special treatment because of the limited resolution of the underlying numerical grid in the vicinity of flames. In large scale fire simulations, grid cells are typically on the order of tens of centimeters. Relatively thin flame sheets cannot be resolved, in which case the resolved temperature field will not reflect the true temperatures one would expect to find in the reaction zone. Consequently, the source term is approximated in grid cells where fuel and oxygen react. Elsewhere, there is greater confidence in the resolved temperature field, and the source term can be computed directly as

$$\kappa\,I_b = \begin{cases} \kappa\,\sigma\,T^4/\pi & \text{Outside flame zone} \\ \max(\chi_r\,\dot{q}'''/4\pi \,,\, \kappa\,\sigma\,T^4/\pi) & \text{Inside flame zone} \end{cases} . \tag{19}$$

Here, χ_r is an empirical estimate of the fraction of that energy emitted as thermal radiation. Typically, a sooty fire radiates approximately one-third of the total combustion energy.

The radiation equation is solved using the Finite Volume Method (FVM). Using approximately 100 discrete angles which are updated over multiple time steps, the finite volume solver requires about 20 % of the total CPU time of a calculation, a modest cost given the complexity of radiation heat transfer.

August 29, 2011 9:45 International Journal of Computational Fluid Dynamics McGrat-
tan-IJCFD-Anonymous
Page 11 of 20

International Journal of Computational Fluid Dynamics

International Journal of Computational Fluid Dynamics 11

1
2
3
4
5
6
7
8
9
10
11
12
13
14
15
16
17
18
19
20
21
22
23
24
25
26
27
28
29
30
31
32
33
34
35
36
37
38
39
40
41
42
43
44
45
46
47
48
49
50
51
52
53
54
55
56
57
58
59
60

3.6.3. *Surface Heat Transfer*

In fires, the temperature solution inside the gas phase is tightly coupled to the temperatures of the surrounding surfaces. Each surface cell can be associated with a one-dimensional solver of heat conduction, internal radiation and thermal degradation inside a condensed material. This solver provides the temperature and species mass flux boundary conditions to the gas phase solution.

$$\rho_s c_s \frac{\partial T_s}{\partial t} = \frac{\partial}{\partial x} k_s \frac{\partial T_s}{\partial x} + \dot{q}_{s,c}''' + \dot{q}_{s,r}''' \tag{20}$$

where ρ_s, k_s and c_s are the temperature dependent density, conductivity and specific heat of the material mixture, and $\dot{q}_{s,c}'''$ and $\dot{q}_{s,r}'''$ are the chemical and radiative source terms, respectively. Specification of appropriate reaction schemes and model parameters for the real-world materials has become an active research topic within the fire community.

4. Solution Procedure

For each grid cell at the nth time step, we have the density, ρ^n, lumped species mass fractions, Z_α^n, velocity vector, $\mathbf{u}^n$, and perturbation pressure term, $\mathcal{H}^n$. In addition, for each compartment in the computational domain, we have a background pressure, $\bar{p}^n$. The temperature is found from the equation of state. These variables are advanced in time using an explicit second-order predictor/corrector scheme. The basic procedure is as follows:

4.1. *Predictor Stage*

(1) Estimate ρ, Z_α, and $\bar{p}$ at the next time step with an explicit Euler step. For example, the density is estimated by:

$$\frac{\rho^* - \rho^n}{\delta t} + \nabla \cdot \rho^n \mathbf{u}^n = 0. \tag{21}$$

The asterisk denotes a first-order accurate estimate at the next time step. Note that the source term is time-split (Corrector Step 2).

(2) Compute the divergence, $(\nabla \cdot \mathbf{u})^*$, from Eq. (10) using the estimated thermodynamic quantities. Note that we use the parentheses to emphasize that an estimate of the velocity field, $\mathbf{u}^*$, at the next time step has not been computed yet, only its divergence.

(3) Solve the Poisson equation for the pressure term:

$$\nabla^2 \mathcal{H}^n = -\frac{(\nabla \cdot \mathbf{u})^* - \nabla \cdot \mathbf{u}^n}{\delta t} - \nabla \cdot \mathbf{F}^n. \tag{22}$$

(4) Estimate the velocity at the next time step:

$$\frac{\mathbf{u}^* - \mathbf{u}^n}{\delta t} + \mathbf{F}^n + \nabla \mathcal{H}^n = 0. \tag{23}$$

12

Note that this procedure guarantees that the divergence of the estimated velocity field, $\nabla \cdot \mathbf{u}^*$, is identically equal to the divergence that is derived from the estimated thermodynamic quantities, $(\nabla \cdot \mathbf{u})^*$, in Step (2).

(5) Check that the time step, δt, satisfies the CFL and Von Neumann stability conditions:

$$\delta t \left(\frac{|u|}{\delta x} + \frac{|v|}{\delta y} + \frac{|w|}{\delta z} \right) < 1 \quad ; \quad 2 \, \delta t \, \frac{\mu}{\rho} \left(\frac{1}{\delta x^2} + \frac{1}{\delta y^2} + \frac{1}{\delta z^2} \right) < 1. \quad (24)$$

If the time step is too large, it is reduced so that it satisfies both constraints and the procedure returns to the beginning of the time step. If the time step satisfies the stability criteria, the procedure continues to the corrector step.

4.2. *Corrector Stage*

(1) Correct ρ, Z_α, and $\overline{p}$ at the next time step. For example, the density is corrected:

$$\frac{\rho^{**} - \frac{1}{2} \left(\rho^n + \rho^* \right)}{\delta t/2} + \nabla \cdot \rho^* \mathbf{u}^* = 0. \quad (25)$$

Z_α, and $\overline{p}$ are corrected in a similar way. The temperature is obtained from the equation of state.

(2) *Time splitting for mass source terms.* After the corrector step for the transport scheme, source terms are applied to the scalars. The source terms are evaluated using the results from the corrected scalar transport scheme:

$$\frac{(\rho Y_\alpha)_{ijk}^{n+1} - (\rho Y_\alpha)_{ijk}^{**}}{\delta t} = \dot{m}_{\alpha,ijk}'''(\mathbf{Y}^{**}, T^{**}). \quad (26)$$

(3) Compute the divergence, $(\nabla \cdot \mathbf{u})^{n+1}$, from the corrected thermodynamic quantities.

(4) Compute the pressure term using the estimated quantities:

$$\nabla^2 \mathcal{H}^* = - \left[\frac{(\nabla \cdot \mathbf{u})^{n+1} - \frac{1}{2} \left(\nabla \cdot \mathbf{u}^* + \nabla \cdot \mathbf{u}^n \right)}{\delta t/2} \right] - \nabla \cdot \mathbf{F}^*. \quad (27)$$

(5) Correct the velocity at the next time step:

$$\frac{\mathbf{u}^{n+1} - \frac{1}{2} \left(\mathbf{u}^* + \mathbf{u}^n \right)}{\delta t/2} + \mathbf{F}^* + \nabla \mathcal{H}^* = 0. \quad (28)$$

Note again that the divergence of the corrected velocity field is identically equal to the divergence that was computed in Step (3).

International Journal of Computational Fluid Dynamics 13

5. Model Validation

The single most important quantity of any fire scenario is the heat release rate (HRR):

$$\dot{Q} = \int \dot{q}''' \, dV \tag{29}$$

In fact, when fire protection engineers talk about the "size" of the fire, they are referring to its HRR rather than its physical dimensions. The "fire plume" is the most fundamental fire-driven flow, encompassing both the visible flames and the thermal, smoke-laden plume. The most important test of a fire model, therefore, is to simulate a fire plume; predicting the height of the visible flames, its centerline velocity and temperature, and its pulsation frequency.

5.1. *Flame Height*

To assess the model's prediction of flame height, we need to look at a wide array of fires. An experimental correlation for flame height, L_f, is given by Heskestad (1983):

$$\frac{L_f}{D} = 3.7 \, (Q^*)^{2/5} - 1.02 \tag{30}$$

where

$$Q^* = \frac{\dot{Q}}{\rho_\infty \, c_p \, T_\infty \, \sqrt{g} \, D^{5/2}} \tag{31}$$

is a non-dimensional quantity that relates the fire's heat release rate, $\dot{Q}$, with the diameter of its base, D. The greater the value of Q^*, the higher the flame height relative to its base diameter. Q^* is sometimes referred to as the fire Froude number. The correlation has been experimentally validated for a range $0.1 < Q^* < 10000$, which represent fires ranging from a lazy camp fire to an oil well blowout. Figure 1 compares the FDS predictions with Heskestad's empirical correlation. Note that the flame height for the FDS simulations is defined as the distance above the pan, on average, at which 99 % of the fuel has been consumed. Note also that the simulations were run at three different grid resolutions. A convenient length scale is given by

$$D^* = \left(\frac{\dot{Q}}{\rho_\infty \, c_p \, T_\infty \, \sqrt{g}} \right)^{2/5} . \tag{32}$$

Given a grid cell size, δx, the three resolutions can be characterized by the non-dimensional quantity, $D^*/\delta x$, whose values in this case are 5, 10 and 20. A simulation where the characteristic diameter of the fire is spanned by only 5 grid cells might be considered poorly resolved, but it is not unusual in a practical fire protection design application where the overall volume of the enclosure may be much larger than that of the fire plume.
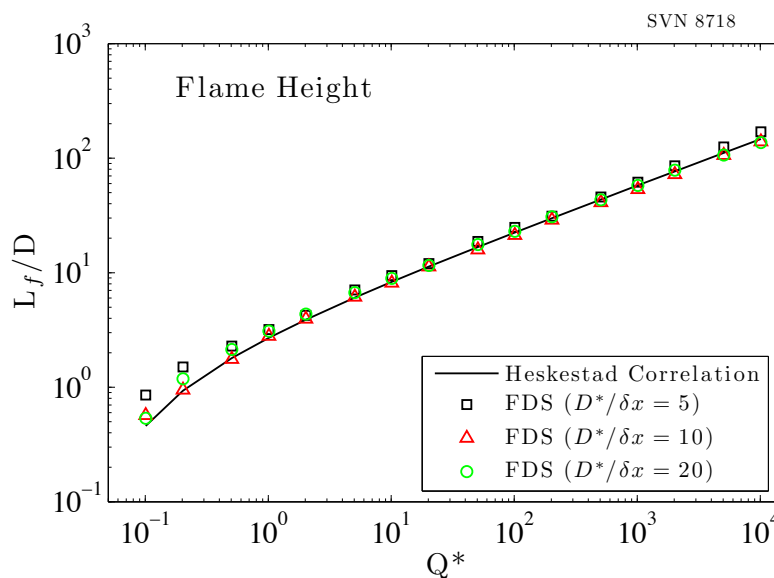
14

Figure 1. Comparison of FDS predictions of flame height from a 1 m square pan fire for Q*
values ranging from 0.1 to 10000.

5.2. *Puffing Frequency*

Figure 2 displays sequential flame images for a single puff from a simulation of a 1 m
methane fire experiment (Test 17) conducted at Sandia National Laboratories (Tieszen
et al. 2002). This is a well-resolved calculation, with $\delta x = 1.5$ cm ($D^*/\delta x = 100$). To
determine the puffing frequency, we record a time series of the vertical component of
velocity along the plume centerline half a diameter from the base (this is the same
location of the velocity measurement used to determine the puffing frequency in the
Sandia experiment). The power spectrum of the signal, taken between 10 s and 20 s from
the simulation, is plotted in Fig. 3. The dominant puffing mode shows good agreement
with the measured puffing frequency of 1.65 Hz, denoted by the vertical dashed line.
Higher frequency fluctuations from the simulation exhibit the classic -5/3 scaling of
Kolmogorov turbulence (Pope 2000). The noise in the spectrum is due to the short
time window (10 s). The spectrum is truncated due to output resolution (the frequency
at which we sample the velocity in the simulation). The temporal Nyquist limit of the
simulation (half the inverse of the time step) is roughly 200 Hz for this case, which means
that the -5/3 scaling is physical, not fortuitous numerical noise.

6.   Practical Applications

Given the importance of the heat release rate (HRR) in fire science, it is not surprising
that the fire scenarios analyzed by the model fall into two classes: those for which the
HRR is *specified* as an input to the model and those for which the HRR is *predicted* by
the model. The former is often the case for a design application, the latter for a forensic
reconstruction.

1
2
3
4
5
6
7
8
9
10
11
12
13
14
15
16
17
18
19
20
21
22
23
24
25
26
27
28
29
30
31
32
33
34
35
36
37
38
39
40
41
42
43
44
45
46
47
48
49
50
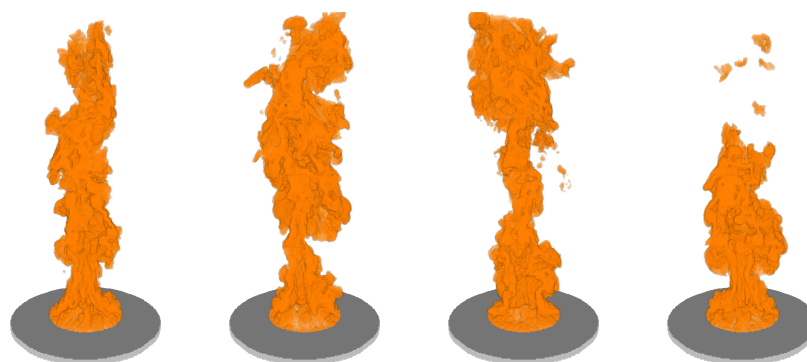51
52
53
54
55
56
57
58
59
60

Figure 2. Snapshots of the flame envelop from a simulation of the Sandia 1 m diameter methane pool fire using 1.5 cm grid resolution. The images span a single "puff".
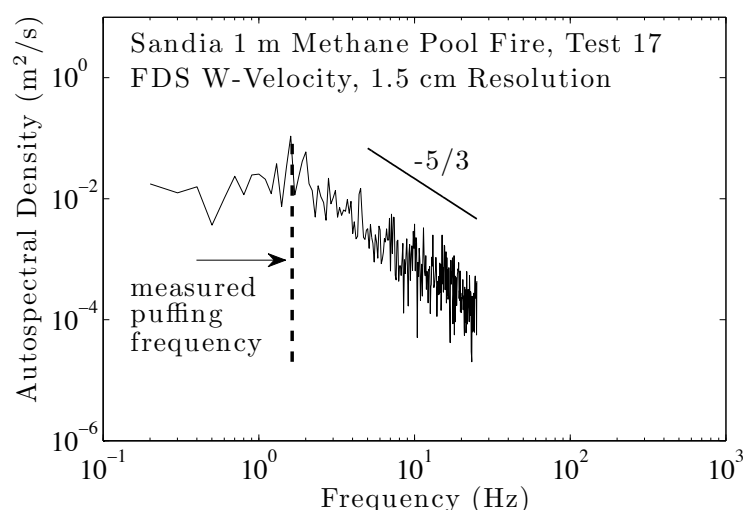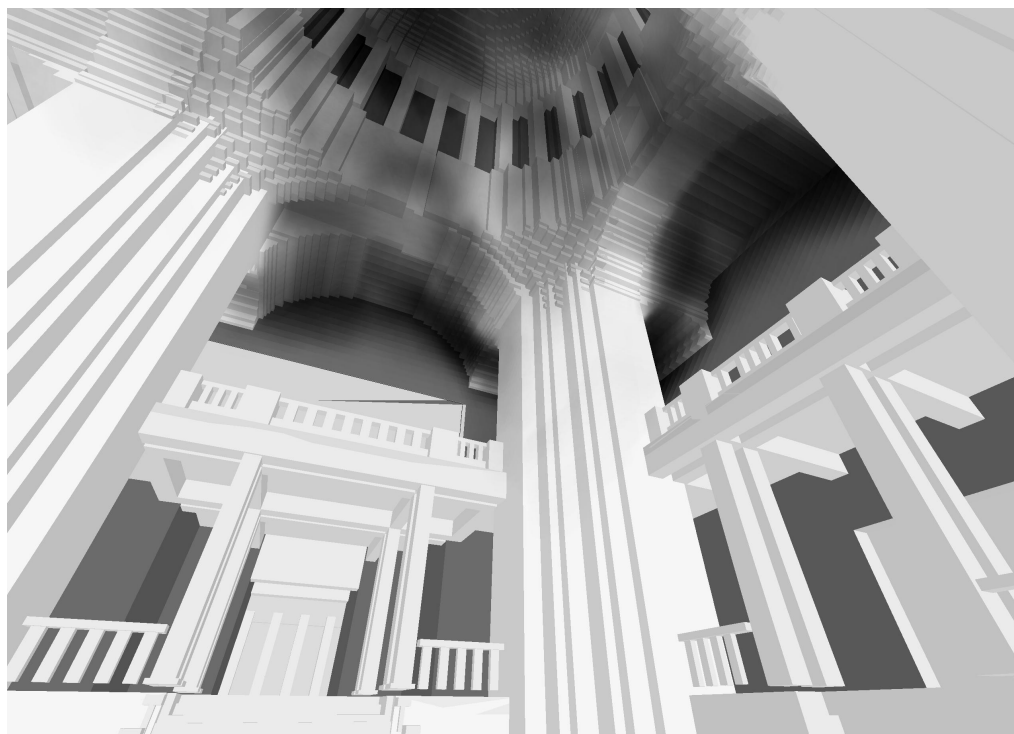

Figure 3. FDS power spectrum for the Sandia 1 m diameter methane pool fire. The dominant mode of the power spectrum from the simulation agrees well with the experimentally measured puffing frequency of 1.65 Hz. The higher frequency fluctuations from the simulation exhibit the classic -5/3 scaling of Kolmogorov turbulence (Pope 2000).

6.1. *Fire Protection Design*

Design applications typically involve an existing building or a building under design. A so-called "design fire" is specified either by a regulatory authority or by the engineers performing the analysis. Because the fire's HRR is specified, the role of the model is to predict the transport of heat and combustion products throughout the space of interest. Ventilation equipment such as fans, blowers, exhaust hoods, heating ducts, and smoke management systems are often included in the simulation. Sprinkler and heat and smoke detector activation are also of interest. The effect of the sprinkler spray on the fire is usually of less interest since the heat release rate of the fire is specified rather than predicted. Detailed descriptions of the contents of the building are usually not necessary

16

because these items are assumed not to contribute to the fire. Even if they do contribute, their burning rate will be specified, not predicted. Sometimes, it is necessary to predict the heat flux from the fire to a nearby "target," and even though the target may heat up to some specified ignition temperature, the subsequent spread of the fire usually goes beyond the scope of the analysis because of the uncertainty inherent in object-to-object fire spread.

Figure 4 displays an example of a fire modeling study. As part of the modernization of the Rhode Island State House (the rotunda is the fourth largest, self supporting dome in the world), FDS was used to model a number of fire scenarios within the structure. The building supervisors wished to avoid having to disrupt the historical fabric of the rotunda while updating the building's fire protection systems. The model was used to examine a number of fire scenarios and how they might impact the ability of occupants to evacuate the building. Note in Fig. 4 the use of rectangular obstructions to approximate the very complicated geometry of the building—a simple alternative to a more CPU intensive body-fitted coordinate system. In this case, the numerical grid consists of approximately 1.4 million cells, each 0.4 m on a side. The computational domain spans a volume that is approximately 60 m by 50 m by 30 m high. The calculation was performed on a single processor personal computer, and the run time was on the order of a few days. Although it is possible to run the calculation faster using parallel processing, common practice is to use dedicated single processors to simulate different potential fire scenarios.

Time: 279.6

Figure 4. View from the floor of the rotunda of the Rhode Island State Capitol, looking upwards at smoke emanating from a hallway at the upper level of the building. Courtesy Hughes Associates, Baltimore, Maryland.

1
2
3
4
5
6
7
8
9
10
11
12
13
14
15
16
17
18
19
20
21
22
23
24
25
26
27
28
29
30
31
32
33
34
35
36
37
38
39
40
41
42
43
44
45
46
47
48
49
50
51
52
53
54
55
56
57
58
59
60

6.2.   *Fire Reconstructions*

Forensic reconstructions require the model to simulate an actual fire based on information that is collected after the event, such as eye witness accounts, unburned materials, and burn signatures. The purpose of the simulation is to connect a sequence of discrete observations with a continuous description of the fire dynamics. Usually, reconstructions involve more gas/solid phase interaction because virtually all objects in a given room are potentially ignitable. Thus, there is much more emphasis on such phenomena as heat transfer to surfaces, pyrolysis, flame spread, and suppression. In general, forensic reconstructions are more challenging simulations to perform because they require more detailed information about the room contents, and there is much greater uncertainty in the total heat release rate as the fire spreads from object to object. The two most notable examples of fire reconstructions by NIST using FDS were the fires within different buildings of the World Trade Center on September 11, 2001 (McGrattan *et al.* 2005); and the Station Nightclub Fire in Rhode Island in February, 2003 (Grosshandler *et al.* 2005).

Fire reconstructions are a combination of numerical simulation and small, medium and large-scale experimentation. Small-scale experiments are conducted to measure the thermo-physical properties of the furnishings, carpeting, and equipment that are assumed to have played a major role in causing or spreading the fire. Medium-scale experiments are conducted to measure the burning rates of individual pieces of furniture. Large-scale experiments are conducted to measure the heat release rate and temperature within compartments that are characteristic of the actual building under study. The small and medium-scale experiments provide input data for the model. The large-scale experiments determine if the model has the necessary physics to describe the behavior of the fire. For example, Fig. 5 shows a photograph of an experiment that was designed to replicate the fire conditions within the two towers of the World Trade Center. The adjacent plot shows the measured and predicted heat release rate of the fire. The simulation was
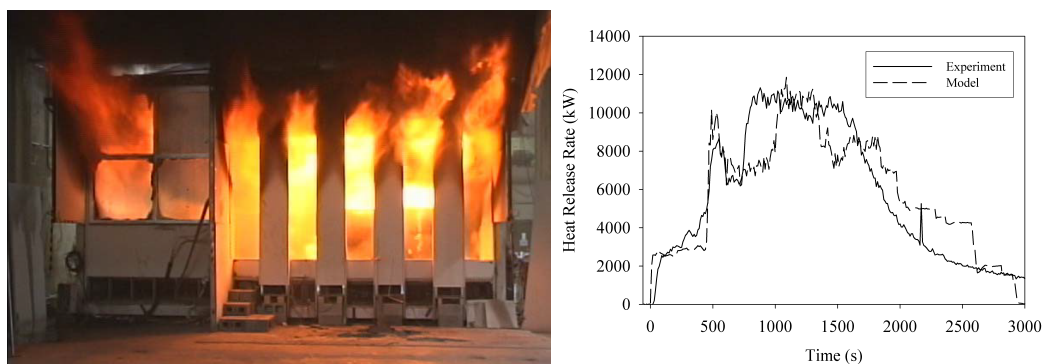

Figure 5.   (Left) Fire experiment conducted in support of the investigation of the collapse of the World Trade Center. (Right) Comparison of predicted and measured heat release rate of the fire.

performed before the experiment, but the model representation of the office furnishings within the compartment were based on bench-scale measurements of material properties and medium-scale burns of individual office workstations. In other words, the prediction is not based solely on material properties derived from bench-scale measurements. Thus, this is not a true validation exercise, but rather one in which the model is calibrated based on small and medium-scale experiments. The model is then shown to predict the fire behavior at the scale of interest. Assuming that the model adequately describes the

18

1
2
3
4
5
6
7
8
9
10
11
12
13
14
15
16
17
18
19
20
21
22
23
24
25
26
27
28
29
30
31
32
33
34
35
36
37
38
39
40
41
42
43
44
45
46
47
48
49
50
51
52
53
54
55
56
57
58
59
60

fire behavior, it is then used to simulate the actual fire event. Figure 6 displays the movement of the fire over two floors of WTC 1 (the north tower) for the period of time between airplane impact and collapse. The purpose of the calculations was to provide the thermal boundary conditions for the structural models that were used to identify the collapse sequence. The large-scale compartment experiments confirmed the model's ability to predict the temperatures of such a fire.
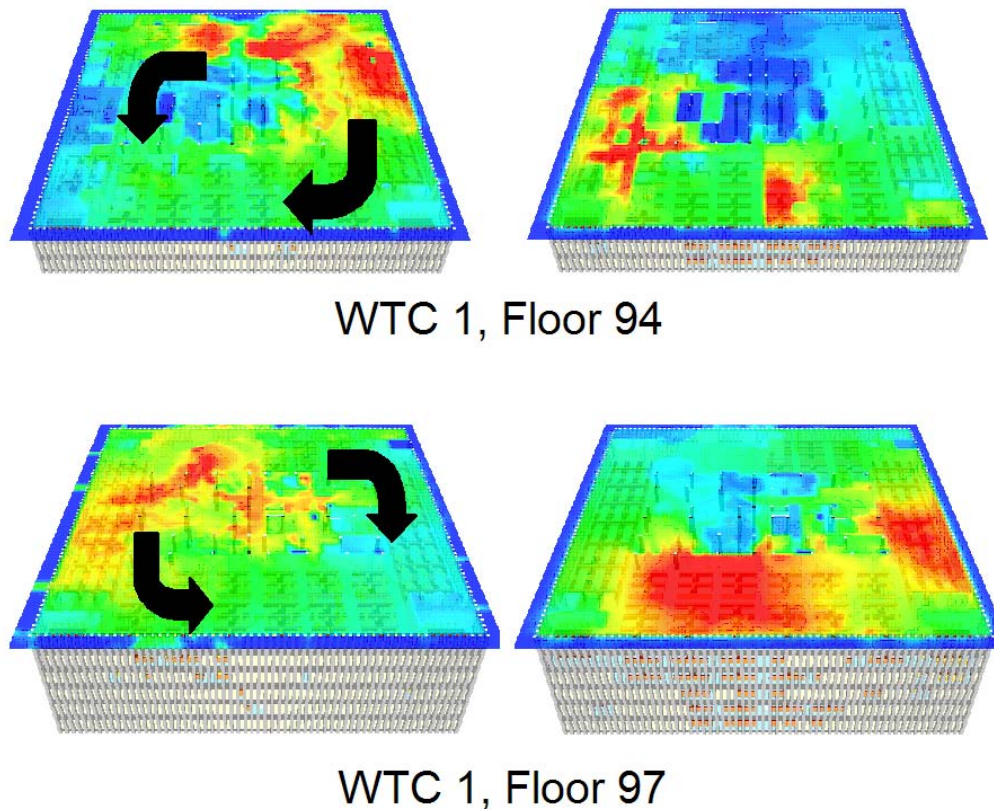

Figure 6. Movement of the fires over two floors of WTC 1, the north tower of the World Trade Center. Shown are contours of the gas temperatures just below the ceiling. The gas temperature history at each point provided boundary conditions for structural models that were used to identify the collapse sequence.

7. Conclusion

CFD modeling of fire has made tremendous progress over the past few decades as our understanding of fire improves and as computers have become ever faster. Current generation models address transport phenomena reasonably well, making them useful for many engineering applications. In fact, it is now common practice for architects to design buildings using three-dimensional computer aided design (CAD) software, and fire

protection engineers have developed ways to extract the necessary geometrical informa-
tion from these programs (Dimyadi *et al.* 2008). The use of simple rectilinear grids and
immersed boundary methods will enable fire models to utilize the same set of drawings
as other building systems engineers. This relieves fire model developers of the burden of
designing sophisticated graphical user interfaces (GUI) themselves. Moving forward, the
modeling of smoke and heat transport within complicated spaces will benefit from the
improvement in large-eddy simulation, parallel processing, and computer aided design,
none of which are specific to fire. Indeed, fire protection engineering is a relatively small
field and there are not enough resources to take on these challenges alone.

However, in spite of these improvements in CFD and the transport of smoke and heat,
we have not yet reached the point of reliably predicting, for large scale applications,
such important phenomena as flame spread, extinction, suppression, and CO and smoke
production, all of which demand more detailed chemistry and physics than are currently
incorporated in the models. Work in these areas has focused on relatively small-scale
combustion systems, and more work is needed to apply what is learned to fires that
spread throughout entire buildings. Most important of all—and something that has only
been briefly discussed in this paper—is the behavior of real materials in fire. Common
combustibles like wood and paper are surprisingly difficult to model because there is
nothing like the Navier-Stokes equations for solid phase decomposition and pyrolysis.
That is, there is no single treatment of real materials that has universal acceptance in
the field. Future developments in fire modeling will focus more on the solid phase, with
steady improvements to the description of combustion in less than ideal environments.
From the standpoint of CFD, solid surfaces are merely boundary conditions, but progress
in CFD modeling of fire cannot advance further until the mathematical description of
real materials reaches the same level of fidelity as that of the gas phase.

References

Dimyadi, J., Spearpoint, M., and Amor, R., 2008. Sharing Building Information using
the IFC Data Model for FDS Fire Simulation. *In: Fire Safety Science—Proceedings
of the Ninth International Symposium*, September. Karlsruhe, Germany.

Germano, M., *et al.*, 1991. A dynamic subgrid-scale eddy viscosity model. *Phys. Fluids
A*, 3 (7), 1760–1765.

Grosshandler, W., RadCal: A Narrow Band Model for Radiation Calculations in a Com-
bustion Environment. , 1993. , NIST Technical Note TN 1402, National Institute of
Standards and Technology, Gaithersburg, Maryland.

Grosshandler, W., *et al.*, Report of the Technical Investigation of The Station Nightclub
Fire. , 2005. , NIST NCSTAR 2, National Institute of Standards and Technology,
Gaithersburg, Maryland.

Harlow, F.H. and Welch, J.E., 1965. Numerical calculation of time-dependent viscous
incompressible flow of fluid with a free surface. *Phys. Fluids*, 8, 2182.

Heskestad, G., 1983. Luminous Heights of Turbulent Diffusion Flames. *Fire Safety Jour-
nal*, 5, 103–108.

Hottel, H., 1984. Stimulation of Fire Research in the United States After 1940 (A His-
torical Account). *Combustion Science and Technology*, 39, 1–10.

Jones, W., A Review of Compartment Fire Models. , 1983. , NBSIR 83-2684, National
Bureau of Standards (now NIST), Gaithersburg, Maryland.

Magnussen, F. and Hjertager, B., 1977. On Mathematical Modeling of Turbulent Com-

20

REFERENCES

bustion with Special Emphasis on Soot Formation and Combustion. *In: Proceedings of the Sixteenth Symposium (International) on Combustion*, 719–729.

McGrattan, K., Bouldin, C., and Forney, G., Federal Building and Fire Safety Investigation of the World Trade Center Disaster: Computer Simulation of the Fires in the WTC Towers. , 2005. , NIST NCSTAR 1-5F, National Institute of Standards and Technology, Gaithersburg, Maryland.

McGrattan, K., *et al.*, Fire Dynamics Simulator, Technical Reference Guide, Volume 3: Experimental Validation. , 2007a. , NIST Special Publication 1018, National Institute of Standards and Technology, Gaithersburg, Maryland.

McGrattan, K., *et al.*, Fire Dynamics Simulator, Technical Reference Guide, Volume 1: Mathematical Model. , 2007b. , NIST Special Publication 1018, National Institute of Standards and Technology, Gaithersburg, Maryland.

Moin, P., *et al.*, 1991. A dynamic subgrid-scale model for compressible turbulence and scalar transport. *Phys. Fluids A*, 3 (11), 2746–2757.

Oran, E. and Boris, J., 1987. *Numerical Simulation of Reactive Flow*. New York: Elsevier Science Publishing Company.

Patankar, S., 1980. *Numerical Heat Transfer and Fluid Flow*. New York: Hemisphere Publishing.

Poinsot, T. and Veynante, D., 2005. *Theoretical and Numerical Combustion*. 2nd Philadelphia, Pennsylvania: R.T. Edwards, Inc.

Pope, S.B., 2000. *Turbulent Flows*. Cambridge.

Quintiere, J., 1984. A Perspective on Compartment Fire Growth. *Combustion Science and Technology*, 39, 11–54.

Rehm, R. and Baum, H., 1978. The Equations of Motion for Thermally Driven, Buoyant Flows. *Journal of Research of the NBS*, 83, 297–308.

Smagorinsky, J., 1963. General Circulation Experiments with the Primitive Equations. I. The Basic Experiment. *Monthly Weather Review*, 91 (3), 99–164.

Sweet, R., 1973. Direct Methods for the Solution of Poisson's Equation on a Staggered Grid. *Journal of Computational Physics*, 12, 422–428.

Tieszen, S.R., *et al.*, 2002. Experimental Study of the Flow Field In and Around A One Meter Diameter Methane Fire. *Combustion and Flame*, 129, 378–391.